OPEN ACCESS

Interfacial Chemical and Mechanical Reactions between Tungsten-Film and Nano-Scale Colloidal Zirconia Abrasives for Chemical-Mechanical-Planarization

ECS Journal of Solid State Science and Technology, 2020 **9** 054001

Interfacial Chemical and Mechanical Reactions between Tungsten-Film and Nano-Scale Colloidal Zirconia Abrasives for Chemical-Mechanical-Planarization

Eun-Bin Seo,[1] Jae-Young Bae,[2] Sung-In Kim,[3] Han-Eol Choi,[3] Young-Hye Son,[3] Sang-Su Yun,[1] Jin-Hyung Park,[4] and Jea-Gun Park[1,3,z]

[1]*Department of Electronics and Communications Engineering, Hanyang University, Seoul 04763, Republic of Korea*
[2]*Department of Energy Engineering, Hanyang University, Seoul 04763, Republic of Korea*
[3]*Department of Nanoscale Semiconductor Engineering, Hanyang University, Seoul 04763, Republic of Korea*
[4]*UB Materials Inc., Gyeonggi-do 17162, Republic of Korea*

In tungsten (W) film chemical-mechanical-planarization (CMP), the chemical and mechanical reaction behaviors of the W film surface play a critical role in the CMP performance, as determined by oxidation (i.e.,WO_3), corrosion (i.e., WO_4^{2-}), and the electrostatic force at the interface between abrasives and the surface. Unlike a conventional catalyst (i.e., $Fe(NO_3)_3$) for a Fenton reaction in a CMP slurry, a new catalyst ((i.e., potassium ferric oxalate: $K_3Fe(C_2O_4)_3$)) and a new nano-scale (i.e., 23 nm in diameter) abrasives (i.e., Zirconia:ZrO_2) provides specific CMP performance behavior: the maximum W-film polishing rate and a corrosion-free surface are achieved at a specific catalyst concentration (0.03 wt%), and the number of remaining abrasives adsorbed on the W film surface after CMP decreases with increasing concentration of the $K_3Fe(C_2O_4)_3$. These CMP performance characteristics are associated with the following results: (i) The degrees of two different CMP mechanisms (oxidation-dominant or corrosion-dominant) determine the corrosion-free surface of W film. (ii) The dependency of the electrostatic force at the interface between abrasives and the film on the $K_3Fe(C_2O_4)_3$ concentration determines the polishing rate. Finally, (iii) the zeta potential distribution at the interface between the abrasives and the film directly affects the number of remaining abrasives on the surface after CMP.

 [DOI: 10.1149/2162-8777/ab915c]

Manuscript submitted March 18, 2020; revised manuscript received April 20, 2020. Published May 18, 2020.

Supplementary material for this article is available online

Recently, dynamic random access memory (DRAM) and NAND flash memory cells fabricated with an n-type metal-oxide-semiconductor field-effect transistor (n-MOSFETs) and selector have been scaled down below 20 nm.[1,2] In addition, n-MOSFETs for application processor (AP) and CPU devices have been scaled down below 3 nm.[3] Integration of such memory cells and n-MOSFETs in APs and CPUs essentially requires tungsten (W) wiring and plugs. In particular, the number of W wiring and plugs in DRAM, NAND flash memory, AP, and CPU devices has been rapidly increasing as memory cells and n-MOSFETs have been continuously scaled down.[4,5] Furthermore, an n-MOSFET with a W buried-gate structure in DRAM below 20 nm has been introduced to overcome the short-channel effect.[6] Such W buried-gate n-MOSFETs and W wiring and plugs have been fabricated through nanometer-scale W film deposition on a buried gate with a trench structure and a metal line and plug with a damascene structure, followed by W-film chemical-mechanical-planarization (CMP). In particular, the critical parameters of the W-film CMP performance are a higher polishing rate for the bulk W film, the polishing rate selectivity between the W and SiO_2 films and a barrier layer such as a TiN film, a complete lack of dishing and erosion of the remaining W film after CMP, and less abrasive adsorption on the surface of the remaining film. Thus, the understanding of the chemical and physical reaction behavior at the interface between the W-film surface and colloidal abrasives in a CMP slurry has been extremely important for future coming nano-scale semiconductor devices.

Kauffman et al reported that the W-film CMP is performed by a circulation mechanism. This mechanism produces tungsten oxide (WO_3) by oxidizing the W film surface with an oxidant and a catalyst, mechanically polishes the WO_3 by rubbing at the interface between the abrasives and the W-film surface, and then forms and polishes the WO_3 again and again; this is called chemical-mechanical dominant CMP.[7,8] The formation of the WO_3 layer on the W film surface is an important factor in determining the W-film polishing rate, surface roughness after CMP[9,10] and preventing dishing, and it strongly depends on the colloidal abrasive material and Fenton reaction between the oxidant and catalyst in the CMP slurry.[11–14] Note that the slurry for W-film CMP consists of colloidal abrasives, an oxidant, a catalyst, a stabilizer, an inhibitor, a pH titrant, and deionized water (DIW). In general, colloidal silica has been used as an abrasive in CMP slurry, H_2O_2 has been commonly used as an oxidant,[12,13,15,16] and iron(III) nitrate ($Fe(NO_3)_3$)[11,17–21] and potassium ferricyanide ($K_3Fe(CN)_6$)[13,22,23] have been widely used as a catalyst. In particular, those catalysts chemical reacted with the H_2O_2 oxidant, which provokes a violent Fenton reaction,[24–27] increasing the temperature of the slurry and effervescing it.[28] Note that Fenton reaction is an exothermal chemical reaction so as to enhance greatly the decomposition of the H_2O_2 oxidant into H_2O and soluble oxygen in the slurry via chemical reaction between ferric catalyst and H_2O_2 oxidant, increasing the W-film polishing-rate. In addition, the catalyst concentration must be sufficiently high, i.e., greater than 0.1 wt%, to obtain a sufficiently high W-film polishing rate. Unfortunately, such a relatively high catalyst and a high oxidizer concentration can easily induce corrosion of the W-film surface[9] and agglomeration of abrasives with the bubbles via a Fenton reaction, leading to poor stability of CMP slurry with an oxidant (i.e., H_2O_2). In contrast, a lower catalyst concentration leads to better stability.[28]

To solve these problems, we introduce a new ternary catalyst, potassium ferric oxalate ($K_3Fe(C_2O_4)_3$), which provokes less of Fenton reaction by being ionized to K^{3+} and $[Fe(C_2O_4)_3]^{3-}$ in an aqueous solution as shown in Supplementary Fig. S1 available online at stacks.iop.org/JSS/9/054001/mmedia, which has not been reported yet. Moreover, to prevent dishing in W-film CMP, we applied a mechanically dominant CMP approach using nanocrystalline colloidal-zirconia (ZrO_2) abrasives in the slurry, which has not been reported either. The W-film surface is considerably hard; i.e.,

[z]E-mail: parkjgL@hanyang.ac.kr

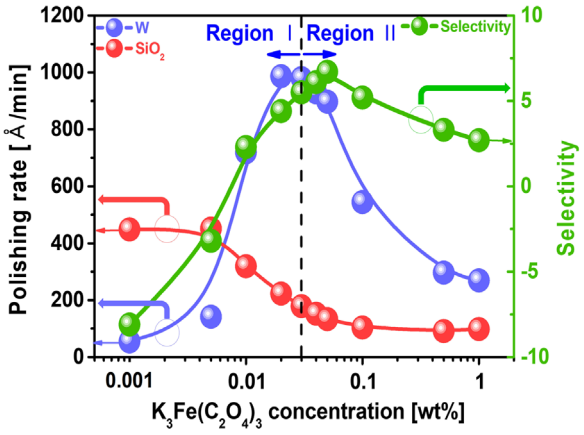

Figure 1. Dependencies of the W-film polishing rate, SiO_2-film polishing rate, and polishing-rate selectivity between the films on the $K_3Fe(C_2O_4)_3$ catalyst concentration.

Mohs hardness of 7.5 GPa. Hence, the W-film surface should be chemically oxidized by forming a WO_3 layer on the W-film surface, resulting in a softer W-film surface (i.e., Mohs hardness of 5.0–-7.0 GPa). So as to enhance W-film polishing rate, a harder abrasive such as colloidal crystalline ZrO_2 (i.e., Mohs hardness of 8.0 GPa) would be essentially necessary, compared to colloidal amorphous SiO_2 (i.e., Mohs hardness of 6.0–7.0 GPa). Thus, for W-film CMP using nanocrystalline colloidal-ZrO_2 abrasives in the slurry, we investigated the dependency on the $K_3Fe(C_2O_4)_3$ catalyst concentration of the W-film CMP performance, including the W- and SiO_2-film polishing rates, the polishing-rate selectivity between the W and SiO_2 films, the static etch rate (SER) of the W film, the surface morphology and roughness, and colloidal abrasive adsorption on the W and SiO_2 film surfaces. In particular, in order to understand surface chemical and mechanical reaction at interface between W-film and nanoscale colloidal-ZrO_2 abrasives for CMP using $K_3Fe(C_2O_4)_3$ catalyst, the dependency mechanism of the W-film CMP performance on the $K_3Fe(C_2O_4)_3$ concentration was analyzed in terms of the film characterization of the W film surface as obtained by X-ray photoelectron spectroscopy (XPS), the corrosion potential and current obtained using a potentiostat, and the zeta potentials of the nanocrystalline ZrO_2 colloidal-abrasives, SiO_2 film surface, and W film surface, obtained using a particle analyzer.

Materials and methods

Materials.—The slurry used in this study consisted of abrasives, a pH titrant, an oxidant (H_2O_2), a catalyst, and DIW. The abrasives were nanocrystalline colloidal-zirconia (ZrO_2) particles with an average primary diameter size of approximately 23 nm. They had a rounded crystalline fringe and a monoclinic crystal structure. The concentrations of the colloidal abrasives and the oxidant were fixed at 1.2 and 1.5 wt%, respectively. A concentration of 0.2 wt% of an anionic polymeric dispersant of the polycarboxylic-acid type was added to disperse the abrasives in the DIW through stirring. Various slurries with different $K_3Fe(C_2O_4)_3$ concentrations (0.001–1.0 wt%) were prepared. All slurries were titrated to pH 2.3 with HNO_3.

Methods.— *CMP conditions.*—To investigate the CMP performance, we prepared two groups of 8-inch wafers: the first group had a structure of Si substrate/SiO_2 (100 nm)/TiN (100 nm)/W (600 nm), and the second one had a structure of Si substrate/SiO_2 (700 nm). Then, the 8-inch wafers were cut into 6 cm × 6 cm square samples, which were polished by using a polisher (POLI-300, G&P Technology) with a CMP pad (IC 1000/Suba IV, Rohm and Haas Electronic Materials). The polishing pressure, wafer-carrier rotation speed, and table rotation speed were 6 psi, 70 rpm, and 70 rpm, respectively. The slurry flow rate was 100 ml min^{-1}. The polishing time for both W and SiO_2 films was 60 s.

Film characterization.—All coupon wafers were rinsed by DIW and dried by nitrogen gas. To calculate the polishing rate, we measured the sheet resistance of the W film by using a four-point probe and the thickness of the SiO_2 film by ellipsometry. The surface morphology of the W film after polishing and static etch was observed by field-emission scanning electron microscopy (FE-SEM) at a 15-kV accelerating voltage. The surface roughness [i.e., an average root mean square (RMS) roughness and peak to peak value (Rpv)] of the W film after polishing was measured by using an atomic force microscope (AFM) with a 2 μm × 2 μm scan area and 1 Hz scan-rate.

Electrochemical analysis.—The static etch rate (SER) of the W film was measured with a four-point probe after dipping a 2 cm × 2 cm sample with W film into a CMP slurry with H_2O_2 at 70 °C for 3 min. The pad surface temperature arrived to 70 °C when the 12-inch-wafer polishing was performed with 3-psi head pressure so that the SER of the W film was estimated at 70 °C for 3 min, as shown in Supplementary Fig. S2. The electrochemical behavior of the W film was examined by taking potentiodynamic measurements with a potentiostat. The area of W film that was exposed to the slurry was 1 cm^2. The reference electrode and counter electrode used a Ag/AgCl electrode and a built-in Pt-coated mesh.

Zeta-potential and secondary abrasive-size.—The zeta potentials of the ZrO_2 abrasives (i.e., 23-nm in primary abrasive size), tungsten trioxide (WO_3—Sigma Aldrich, <100 nm in particle size) particles, and SiO_2 (SiO_2—Sigma Aldrich, 10 ∼ 20 nm in particle size) particles were analyzed by using a particle analyzer (ELSZ2+, Otsuka Electronics) with electrophoresis techniques and dynamic light scattering. Note that the zeta-potentials of WO_3 and SiO_2 particles approximately represent the zeta-potential of the W- and SiO_2-film surface. The secondary ZrO_2 abrasive-size measured as function of the $K_3Fe(C_2O_4)_3$ concentration (i.e., 0.001 ∼ 1.0 wt%).

Results and Discussion

The CMP process is a dynamic cycling process performing chemical reaction and mechanical rubbing. To understand this dynamic cycling process, the chemical properties (i.e., static etch rate, potentiodynamic polarization, XPS), mechanical properties (i.e., zeta-potential of ZrO_2 abrasives, WO_3− and SiO_2-particles, secondary abrasive-size), the chemical and mechanical properties (i.e., the W- and SiO_2-film polishing rate) were characterized in detail.

Dependency of W- and SiO_2-film polishing-rate on catalyst [i.e., $K_3Fe(C_2O_4)_3$]concentration.—Figure 1 shows the dependency of the CMP performance on the $K_3Fe(C_2O_4)_3$ catalyst concentration in the slurry. The performance was estimated by using slurries mixed with 1.5 wt% of the H_2O_2 oxidant. The polishing rate of the W film was only 55 Å min^{-1} at 0.001 wt% of $K_3Fe(C_2O_4)_3$, but it rapidly increased to 987 Å min^{-1} when the $K_3Fe(C_2O_4)_3$ concentration increased to 0.03 wt%. Then, it decreased abruptly to 300 Å min^{-1} when the $K_3Fe(C_2O_4)_3$ concentration increased to 1.0 wt%. The W-film polishing rate thus peaked at a specific concentration of the $K_3Fe(C_2O_4)_3$ catalyst, i.e., 0.03 wt%. This result completely differs from the dependency of the W-film polishing rate on the concentration of a $Fe(NO_3)_3$ catalyst.[17] Specifically, the W-film polishing rate rapidly increases up to a specific $Fe(NO_3)_3$ concentration and then saturates with further increasing concentration.[17,29] On the other hand, the SiO_2 film's polishing rate was sustained at 448 Å min^{-1} when the $K_3Fe(C_2O_4)_3$ concentration increased from 0.001 to 0.005 wt%. Then, it gradually decreased to 104 Å min^{-1} when the $K_3Fe(C_2O_4)_3$ concentration increased to 0.1 wt%. Finally, it saturated at 91 Å min^{-1} with further increasing $K_3Fe(C_2O_4)_3$

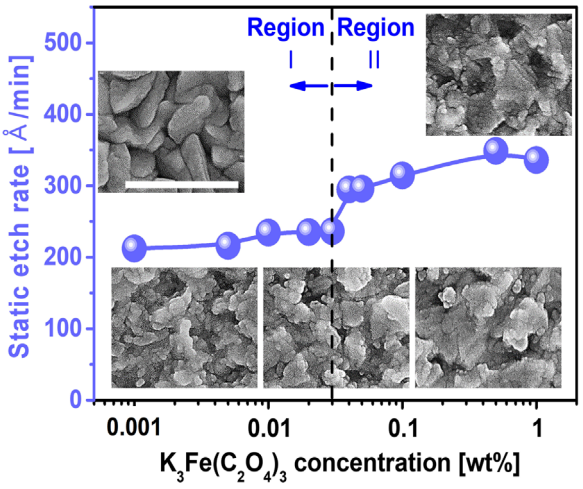

Figure 2. Dependency of the static etch rate (SER) of the W film on the $K_3Fe(C_2O_4)_3$ catalyst concentration. The SEM images of W films after dipping into slurry mixed with the H_2O_2 oxidant were observed at 15 kV.

concentration. As a result, the polishing-rate selectivity between the W and SiO_2 films drastically increased from 0.12:1 to 6.74:1 when the $K_3Fe(C_2O_4)_3$ concentration increased from 0.001 to 0.05 wt%. Then, it slightly decreased to 2.74:1 when the $K_3Fe(C_2O_4)_3$ concentration increased to 1.0 wt%. The selectivity thus peaked at a $K_3Fe(C_2O_4)_3$ concentration of 0.05 wt%.

Dependency of chemical properties (i.e., static etch rate, potentiodynamic polarization, surface chemical reaction) on catalyst [i.e., $K_3Fe(C_2O_4)_3$] concentration.—First of all, to understand the dependency of the CMP performance on the $K_3Fe(C_2O_4)_3$ catalyst concentration in the W-film CMP slurry, we investigated the chemical characteristics (i.e., the SER of the W film surface) after dipping samples into the slurry at 70 °C for 3 min. Figure 2 shows the results as a function of the $K_3Fe(C_2O_4)_3$ concentration in slurries with 1.5 wt% of H_2O_2. Note that CMP performance is determined simultaneously by chemical and mechanical characteristics, and again, that the slurries consisted of nanocrystalline colloidal-ZrO_2 abrasives (1.2 wt%), the $K_3Fe(C_2O_4)_3$ catalyst (0.001–1.0 wt%), the HNO_3 titrant (pH 2.3), and DIW. As seen in region **I** of Fig. 2, the SER of the W film slightly increased from 212 to 236 Å min^{-1} when the $K_3Fe(C_2O_4)_3$ concentration increased from 0.001 to 0.03 wt%. Then, it abruptly increased to 295 Å min^{-1} when the $K_3Fe(C_2O_4)_3$ concentration increased to 0.04 wt%. Afterward, as seen in region **II**, the SER again slightly increased, to 336 Å min^{-1}, when the $K_3Fe(C_2O_4)_3$ concentration increased to 1.0 wt%. This result indicates that the SER of the W film increased with the $K_3Fe(C_2O_4)_3$ concentration via chemical oxidation of the W film surface (giving WO_3) in region **I**, and then it increased with the $K_3Fe(C_2O_4)_3$ concentration via corrosion of the surface in region **II**. This can be seen in the SEM images in Fig. 2, as discussed later in detail.

To confirm the different SER behavior in regions **I** and **II**, we measured potentiodynamic polarization curves for the W film surface as a function of the $K_3Fe(C_2O_4)_3$ concentration. The surface was exposed to slurries with 1.5 wt% of the H_2O_2 oxidant, giving the results shown in Fig. 3. In region **I** [$K_3Fe(C_2O_4)_3$ concentration between 0.001 and 0.03 wt%], the anodic branches showed passivation behavior via oxidation of the W film surface, as indicated by the circle in Fig. 3a. Otherwise, in region **II** [$K_3Fe(C_2O_4)_3$ concentration between 0.04 and 1.0 wt%], the anodic branches presented almost corrosive behavior, indicated by the circle in Fig. 3b. Using the Tafel method, we calculated the corrosion potential (E_{corr}) and corrosion current (I_{corr}) from Figs. 3a and 3b,[30] as shown in Fig. 3c. E_{corr} rapidly increased from 0.199 to 0.366 V when the $K_3Fe(C_2O_4)_3$ concentration increased from 0.001 to 0.005 wt%. It then saturated at ~0.380 V as the $K_3Fe(C_2O_4)_3$ concentration increased to 0.03 wt%. This result means that E_{corr} was enhanced by chemical oxidation of the W film surface (giving WO_3), reaching a value of ~0.380 V. Thus, the surface was chemically oxidized in region **I**. Then, however, E_{corr} gradually decreased to 0.289 V when the $K_3Fe(C_2O_4)_3$ concentration increased to 1.0 wt%. Thus, the W film surface was corroded in region **II**, and the degree of corrosion increased with the $K_3Fe(C_2O_4)_3$ concentration. In addition, I_{corr} slightly decreased from $10^{-4.09}$ to $10^{-4.15}$ A cm^{-2} when the $K_3Fe(C_2O_4)_3$ concentration increased from 0.001 to 0.03 wt%, indicating that the degree of oxidation of the W film surface increased with the $K_3Fe(C_2O_4)_3$ concentration in region **I**. Then, I_{corr} rapidly increased to $10^{-3.74}$ A cm^{-2} when the $K_3Fe(C_2O_4)_3$ concentration increased to 1.0 wt%, meaning that the degree of corrosion the W film surface increased greatly with the $K_3Fe(C_2O_4)_3$ concentration in region **II**.

In summary, the potentiodynamic polarization curve for E_{corr} and I_{corr} in Fig. 3 demonstrates the following: In region **I** [$K_3Fe(C_2O_4)_3$ concentration between 0.001 and 0.03 wt%], the degree of oxidation (giving WO_3) of the W film surface exposed to the slurry at 25 °C increased with the $K_3Fe(C_2O_4)_3$ concentration. In contrast, in region **II** [i.e., $K_3Fe(C_2O_4)_3$ concentration between 0.04 and 1.0 wt%], the degree of corrosion of the W film surface exposed to the slurry at 25 °C increased with the $K_3Fe(C_2O_4)_3$ concentration. Thus, both E_{corr} and I_{corr} peaked at a $K_3Fe(C_2O_4)_3$ concentration of ~0.03 wt %, with respective values of 0.380 V and $10^{-4.15}$ A cm^{-2}. Comparing the dependencies on $K_3Fe(C_2O_4)_3$ concentration shown in Figs. 2 and 3, it is obvious that the SER dependency of the W film surface after dipping into slurry at 70 °C for 3 min correlates well with the E_{corr} and I_{corr} dependency of the W film surface exposed to slurry at 25 °C. Thus, the chemical reaction of the W film surface with slurries including the $K_3Fe(C_2O_4)_3$ catalyst showed oxidation behavior in region **I** but corrosion behavior in region **II**.

To confirm the formation of chemically oxidized WO_3-layer on the W-film surface after CMP, the binding energy of the W-film surface analyzed by XPS. The 4 f 7/2 and 4 f 5/2 peaks of the W-metal were centered at 31.6 and 33.8 eV while those of the WO_3 layer were centered at 35.6 and 37.8 eV,[31] respectively, as shown in Fig. 4a. Both 4 f 7/2 and 4 f 5/2 peaks of the WO_3 layer slightly increased with the $K_3Fe(C_2O_4)_3$ concentration up to 0.03 wt%, i.e., region **I**, and then considerably decreased with increasing $K_3Fe(C_2O_4)_3$ concentration, i.e., region **II**. Otherwise, 4 f 7/2 and 4 f 5/2 peaks of the W-metal slightly decreased with increasing the $K_3Fe(C_2O_4)_3$ concentration up to 0.03 wt%, i.e., region **I**, and then greatly increased with the $K_3Fe(C_2O_4)_3$ concentration, i.e., region **II**. The chemical composition (i.e., chemical binding energy) dependency of the chemically oxidized WO_3-layer on the catalyst $K_3Fe(C_2O_4)_3$ concentration was well correlated with that of potentiodynamic polarization behavior on the catalyst concentration in Fig. 3 as well as that of the W-film polishing rate on the catalyst concentration in Fig. 1.

Dependency of mechanical properties (i.e., electrostatic force and surface topography after CMP) on catalyst [i.e., $K_3Fe(C_2O_4)_3$] concentration..—Here, to understand why the CMP performance, including the W- and SiO_2-film polishing rates, depends on the $K_3Fe(C_2O_4)_3$ catalyst concentration in the W-film CMP slurry, we examined the mechanical characteristics of the CMP process, meaning the electrostatic force at the interface between the W-film surface and the colloidal-ZrO_2. Figure 5 shows the results as a function of the $K_3Fe(C_2O_4)_3$ concentration in the slurries. Each kind of particles was dispersed in slurries with various $K_3Fe(C_2O_4)_3$ concentrations to measure their zeta potentials. Slurries without the H_2O_2 oxidant were titrated to pH 2.3 for measuring zeta potentials of ZrO_2, WO_3, and SiO_2 particles. The ZrO_2 particles corresponded to the colloidal-ZrO_2 abrasives, while the WO_3 and SiO_2 particles represented the chemically oxidized W and SiO_2 film surfaces. The zeta potential of the ZrO_2 particles slightly decreased from +4.55 to

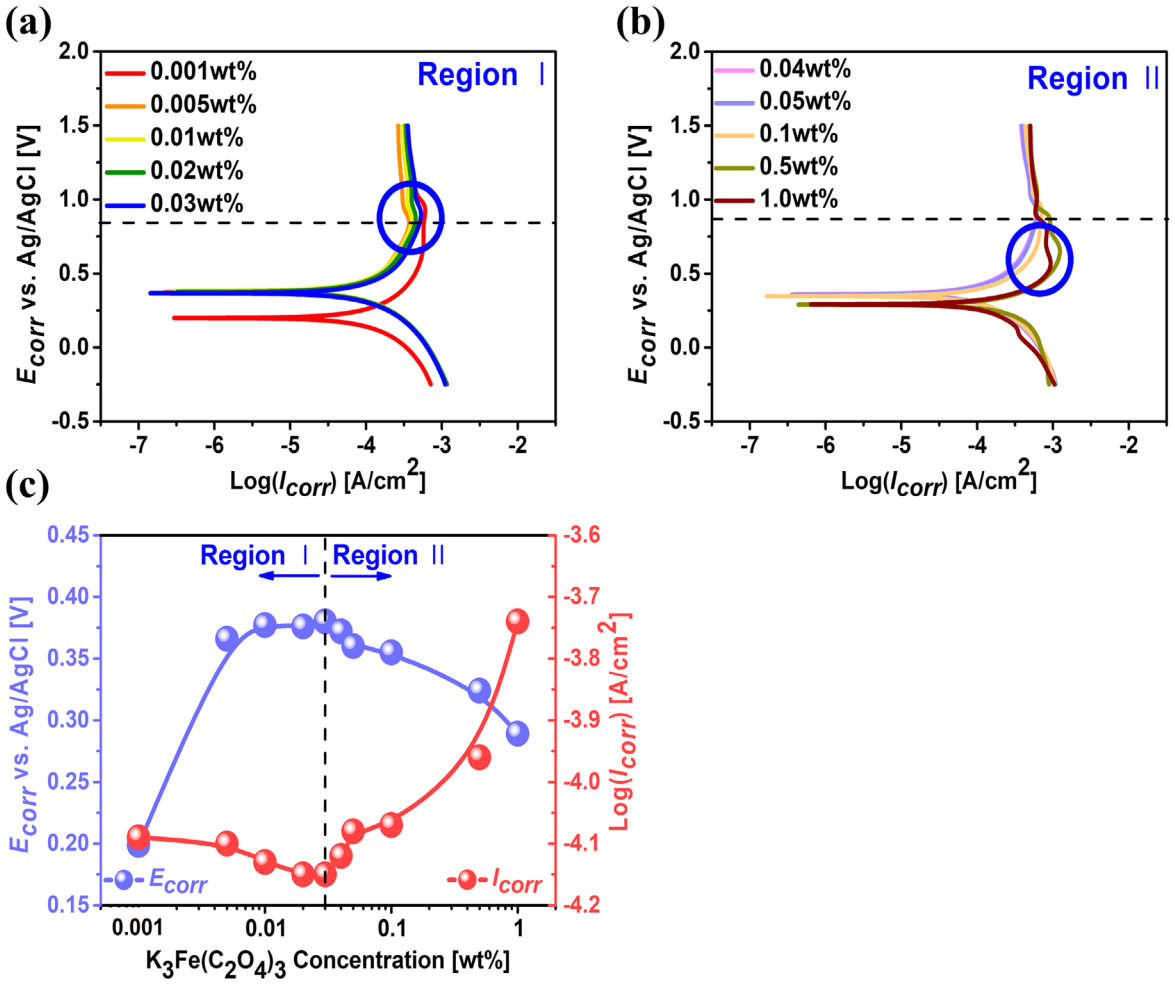

Figure 3. Corrosion potential and current of W-film surfaces exposed to slurry with 1.5 wt% of the H_2O_2 oxidant, as a function of the $K_3Fe(C_2O_4)_3$ catalyst concentration: Potentiodynamic polarization curves of the W-film surface for $K_3Fe(C_2O_4)_3$ concentrations (a) from 0.001 to 0.03 wt% and (b) from 0.04 to 1.0 wt %. (c) Corrosion potential (E_{corr}) and corrosion current density (I_{corr}) of the W-film surface.

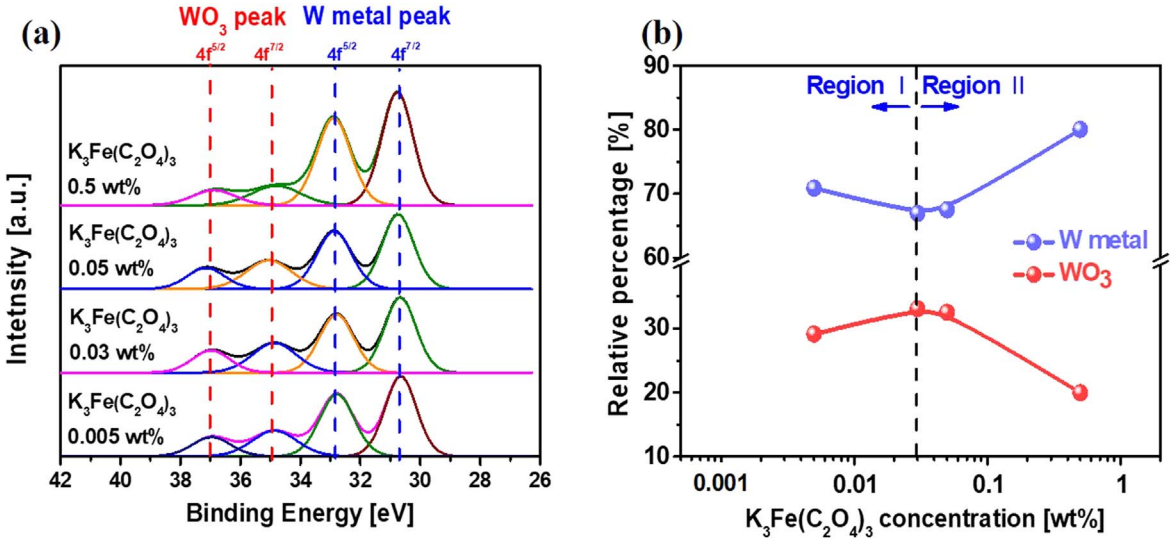

Figure 4. Chemical composition of the W-film surface after CMP analyzed by XPS. (a) Surface spectra intensity vs binding energy and (b) relative percentage vs catalyst $K_3Fe(C_2O_4)_3$ concentration.

+1.32 mV when the $K_3Fe(C_2O_4)_3$ concentration increased from 0.001 to 0.03 wt%, as shown in Fig. 5a.

We can understand this trend by considering the adsorption of $(C_2O_4)^{2-}$ ions on the ZrO_2 particles in the slurry. The $K_3Fe(C_2O_4)_3$ molecules in the slurry decomposed into 3 K^+, Fe^{3+}, and $3(C_2O_4)^{2-}$

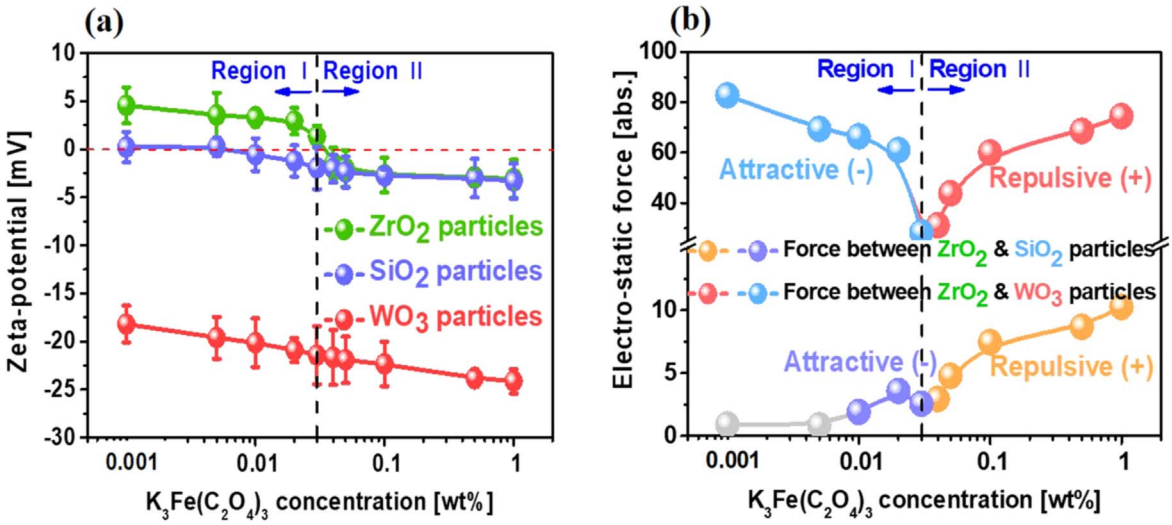

Figure 5. Surface charge distributions of ZrO_2, SiO_2, and WO_3 particles and coulombic force distributions between the ZrO_2 and WO_3 particles and between the ZrO_2 and SiO_2 particles: (a) zeta potentials of the ZrO_2, SiO_2, and WO_3 particle, and (b) electrostatic forces between the ZrO_2 and SiO_2 particles and between the ZrO_2 and WO_3 particles. Particularly, zeta-potentials were measured 4 times.

at pH 2.3, and the zeta potential of the ZrO_2 particles in slurry titrated to pH 2.3 without $K_3Fe(C_2O_4)_3$ was +5.09 mV. Thus, the zeta potential of the ZrO_2 particles in the slurries with $K_3Fe(C_2O_4)_3$ varied from a positive value to a higher negative value as the $K_3Fe(C_2O_4)_3$ concentration increased. In contrast, the zeta potential of the SiO_2 particles became increasingly negative, from +0.20 to −3.32 mV, when the $K_3Fe(C_2O_4)_3$ concentration increased from 0.001 to 1.0 wt%. This trend also can be analyzed by considering the absorption of $(C_2O_4)^{2-}$ ions on the SiO_2 particles. The zeta potential of the SiO_2 particles in slurry titrated to pH 2.3 without $K_3Fe(C_2O_4)_3$ was +0.82 mV. Thus, the zeta potential of the SiO_2 particles in the slurries with $K_3Fe(C_2O_4)_3$ became increasingly negative with increasing $K_3Fe(C_2O_4)_3$ concentration, because a higher $K_3Fe(C_2O_4)_3$ concentration led to higher adsorption of $(C_2O_4)^{2-}$ ions on the SiO_2 particles. The secondary particle-size of the SiO_2 particles in the slurries were sustained with 114 nm even though the $K_3Fe(C_2O_4)_3$ catalyst concentration was varied, implying that the secondary particles in the slurry were very stable. In addition, the zeta potential of the WO_3 particles became considerably more negative, from −18.2 to −24.12 mV, when the $K_3Fe(C_2O_4)_3$ concentration increased from 0.001 to 1.0 wt%. This result can be interpreted by considering both oxidation (giving WO_3) and corrosion (giving WO_4^{2-}) in the slurry. Initially, the zeta potential of the WO_3 particles in slurry titrated to pH 2.3 without the $K_3Fe(C_2O_4)_3$ catalyst was −18 mV. Thus, the zeta potential of the WO_3 particles in the slurries with $K_3Fe(C_2O_4)_3$ became increasingly negative with increasing $K_3Fe(C_2O_4)_3$ concentration, because the degree of corrosion (i.e., the amount of WO_4^{2-}) increased with the $K_3Fe(C_2O_4)_3$ concentration, as explained later in detail.

In CMP, the polishing rate of a film is expressed by the Preston equation:

$$dH/dt = C \cdot p \cdot v,$$

where p and v are the CMP polisher head pressure and the relative velocity between the platen and the head, respectively; and C is a function of the relative electrostatic force between the abrasives and the film, which is calculated from the Coulombic force between particles, pad and abrasive material property and slurry chemistry, etc In general, a weakly attractive (negative) electrostatic force leads to a higher polishing rate, while a strongly repulsive (positive) force leads to a lower polishing rate. From the zeta potentials of the ZrO_2, SiO_2, and WO_3 particles in the slurry [Fig. 5(a)], we calculated the electrostatic force at the interface between the ZrO_2 and WO_3 particles, corresponding to the relative mechanical W-film polishing rate, and the electrostatic force between the ZrO_2 and SiO_2 particles, corresponding to the relative mechanical SiO_2-film polishing rate, as shown in Supplementary Table SI. Figure 5b shows the results. The relative attractive electrostatic force at the interface between the ZrO_2 and WO_3 particles remarkably decreased in absolute value from −82.81 to −28.29 when the $K_3Fe(C_2O_4)_3$ concentration increased from 0.001 to 0.03 wt%. Then, the relative repulsive electro-static force at the interface between the ZrO_2 and WO_3 particles increased greatly from +31.18 to +74.53 when the $K_3Fe(C_2O_4)_3$ concentration increased from 0.04 to 1.0 wt%. This dependency of the electrostatic force at the interface between the ZrO_2 and WO_3 particles on the $K_3Fe(C_2O_4)_3$ concentration correlates with that of the W-film polishing rate on the $K_3Fe(C_2O_4)_3$ concentration, as seen by comparing Fig. 1 with Fig. 5b. In region **I** [$K_3Fe(C_2O_4)_3$ concentration between 0.001 and 0.03 wt%], the W-film polishing rate increased with the $K_3Fe(C_2O_4)_3$ concentration, because the relative attractive (negative) electrostatic force at the interface between the ZrO_2 and WO_3 particles decreased with increasing $K_3Fe(C_2O_4)_3$ concentration. On the other hand, in region **II** [$K_3Fe(C_2O_4)_3$ concentration between 0.04 and 1.0 wt%], the W-film polishing rate decreased with increasing $K_3Fe(C_2O_4)_3$ concentration, because the relative repulsive (positive) electrostatic force at the interface between the ZrO_2 and WO_3 particles increased with the $K_3Fe(C_2O_4)_3$ concentration. Furthermore, the relative electrostatic force at the interface between the ZrO_2 and SiO_2 particles was nearly zero when the $K_3Fe(C_2O_4)_3$ concentration increased from 0.001 to 0.005 wt%. Then, the relative attractive electrostatic force slightly increased in absolute value from 1.91 to 2.57 when the $K_3Fe(C_2O_4)_3$ concentration increased from 0.01 to 0.03 wt%. With further increasing $K_3Fe(C_2O_4)_3$ concentration, the relative repulsive force at the interface between the ZrO_2 and SiO_2 particles slightly increased. This dependency of the electrostatic force at the interface between the ZrO_2 and SiO_2 particles on the $K_3Fe(C_2O_4)_3$ concentration also correlates well with that of the SiO_2-film polishing rate on the $K_3Fe(C_2O_4)_3$ concentration. The polishing rate of the SiO_2 film was about 450 Å min^{-1} at 0.001 and 0.005 wt% $K_3Fe(C_2O_4)_3$, and the electrostatic force was close to zero at the interface between the ZrO_2 and SiO_2 particles. Then, when the $K_3Fe(C_2O_4)_3$ concentration increased from 0.005 to 0.03 wt%, the polishing rate decreased with increasing $K_3Fe(C_2O_4)_3$ concentration, as the relative electrostatic force at the interface between the ZrO_2 and SiO_2 particles became attractive. With further increasing $K_3Fe(C_2O_4)_3$ concentration up to 1.0 wt%, the polishing rate saturated, as the repulsive electrostatic force at the interface between the ZrO_2 and SiO_2 particles was

relatively low. Thus, the dependencies of the W- and SiO_2-film polishing rates on the $K_3Fe(C_2O_4)_3$ concentration correlate well with those of the mechanical characteristics (i.e., the electrostatic forces at the interface between the ZrO_2 abrasives and the SiO_2 and W films) on the $K_3Fe(C_2O_4)_3$ concentration, as seen by comparing Fig. 1 with Fig. 5b. For real CMP, however, we should simultaneously consider the chemical characteristics, as well.

Next, to fully understand the dependency of the CMP performance on the $K_3Fe(C_2O_4)_3$ catalyst concentration in the W-film CMP slurry, we observed the chemical and mechanical characteristics simultaneously. Figure 6 shows the results, which were obtained through SEM and AFM imaging of the surface morphology of the W film surface after CMP. For the as-deposited W film, the surface morphology showed rough, bumpy poly-grains with a size range of 100–300 nm, as seen in Fig. 6a. For the same as-deposited condition, Fig. 6f shows that the root-mean-square (R_q) and peak-to-valley ($R_{p\text{-}to\text{-}v}$) roughnesses of the surface were 13.9 and 97.4 nm, respectively. For the slurry with a $K_3Fe(C_2O_4)_3$ concentration of 0.005 wt%, Fig. 6b shows that the W film surface morphology after CMP presented locally planarized surfaces and locally unpolished poly-grain grooves. This was because the W-film polishing rate was very slow (142 Å min^{-1}) as a result of the lower degree of chemical oxidation (WO_3) of the W film surface. Thus, as shown Fig. 6g, the R_q (8.195 nm) and $R_{p\text{-}to\text{-}v}$ (57.5 nm) of the surface were reduced slightly in comparison to those of the as-deposited surface. Next, for the slurry with a $K_3Fe(C_2O_4)_3$ concentration of 0.03 wt%, the W film surface morphology after CMP exhibited well-planarized surfaces without locally unpolished poly-grain grooves, as shown in Fig. 6c. Here, the W-film polishing rate was sufficiently enhanced (980 Å min^{-1}) by an adequate degree of chemical oxidation of the surface. Thus, as shown in Fig. 6h, the R_q (2.0 nm) and $R_{p\text{-}to\text{-}v}$ (20.3 nm) of the W film surface were reduced remarkably as compared to the case of using the slurry with 0.005 wt% of $K_3Fe(C_2O_4)_3$. In addition, for the slurry with a $K_3Fe(C_2O_4)_3$ concentration of 0.05 wt%, the W film surface after CMP demonstrated almost the same surface morphology, as shown in Fig. 6d. Again, the reason was that the W-film polishing rate was quite high (897 Å min^{-1}) because the degree of chemical oxidation of the W film surface was high enough. Thus, the R_q and $R_{p\text{-}to\text{-}v}$ of the W-film surface were 1.5 and 12.0 nm, respectively, as shown Fig. 6i. For the slurry with a $K_3Fe(C_2O_4)_3$ concentration of 0.5 wt%, however, the W film surface morphology after CMP had sharp, corroded surfaces, as shown in Fig. 6e. This was because the W-film polishing rate was considerably reduced (297 Å min^{-1}) by corrosion of the W film surface. Thus, as shown Fig. 6j, the R_q (11.7 nm) and $R_{p\text{-}to\text{-}v}$ (75.5 nm) of the surface were rather significantly enhanced as compared to the case of using the slurry with 0.05 wt% of $K_3Fe(C_2O_4)_3$.

Comparing Fig. 1 with Figs. 4–6, it is clear that the W-film polishing rate rapidly increased with the $K_3Fe(C_2O_4)_3$ concentration in region **I** [$K_3Fe(C_2O_4)_3$ concentration between 0.001 and 0.03 wt %]. This was because the degree of chemical oxidation of the W film surface was enhanced by the $K_3Fe(C_2O_4)_3$ concentration, while the relative attractive (negative) force at the interface between the nanoscale colloidal-ZrO_2 abrasives and the W film decreased with the increasing $K_3Fe(C_2O_4)_3$ concentration. In contrast, the W-film polishing rate abruptly decreased with increasing $K_3Fe(C_2O_4)_3$ concentration in region **II** [$K_3Fe(C_2O_4)_3$ concentration between 0.04 and 0.1 wt%]. There, the degree of corrosion of the W film surface increased with the $K_3Fe(C_2O_4)_3$ concentration, as did the relative repulsive (positive) electrostatic force at the interface between the ZrO_2 abrasives and the W film. In addition, the chemical characteristics, such as the static etch rate (SER) shown in Fig. 2 and E_{corr} and I_{corr} shown in Fig. 3, also demonstrated the dependency of the surface morphology of the W film after CMP on the $K_3Fe(C_2O_4)_3$ concentration, as seen in Fig. 6. Furthermore, comparing Fig. 1 with Figs. 2–6, for a W film it is evident that there are two different CMP mechanisms when using slurry with the $K_3Fe(C_2O_4)_3$ catalyst: an chemical oxidation-dominant mechanical planarization in region **I** [$K_3Fe(C_2O_4)_3$ concentration between 0.001 and 0.03 wt%], and a corrosion-dominant mechanical planarization in region **II** [$K_3Fe(C_2O_4)_3$ concentration between 0.04 and 0.1 wt%]. Comparing Fig. 1 with Fig. 5 suggests, however, that SiO_2-film CMP has a planarization mechanism dominated by mechanical polishing.

Dependency of CMP mechanism on catalyst [i.e., $K_3Fe(C_2O_4)_3$] concentration.—Next, to understand why chemical oxidation-dominant, corrosion-dominant, and mechanical planarization mechanisms were simultaneously present for the slurries using the $K_3Fe(C_2O_4)_3$ catalyst, we examined the dependency of the surface chemical reaction behavior of W-film CMP on the $K_3Fe(C_2O_4)_3$ concentration. In general, W-film CMP is performed by forming a nanoscale oxide layer (e.g., WO_3) on the W film surface and polishing mechanically at the interface between nanoscale colloidal-ZrO_2 abrasives and the WO_3 layer in an acid region with a pH range of 0–4. This is called the cycling process, as shown in the Pourbaix diagram of Supplementary Fig. S3.[32,33] To form the WO_3 layer, a Fenton reaction[28] between the $K_3Fe(C_2O_4)_3$ catalyst and the H_2O_2 oxidant is necessary for decomposing the H_2O_2 into dissolved O_2 in the aqueous slurry, as shown by the reactions below.

$$K_3Fe(C_2O_4)_3 \rightarrow 3K^+ + Fe^{3+} + 3(C_2O_4)^{2-} \quad [1]$$

$$Fe^{3+} + H_2O_2 \rightarrow FeOOH^{2+} + H^+ \quad [2]$$

$$FeOOH^{2+} \rightarrow Fe^{2+} + HO_2^{\cdot} \quad [3]$$

$$Fe^{2+} + H_2O_2 \rightarrow Fe^{3+} + OH^- + OH^{\cdot} \quad [4]$$

$$OH^{\cdot} + H_2O_2 \rightarrow H_2O + HO_2^{\cdot} \quad [5]$$

$$HO_2^{\cdot} \rightarrow H^+ + O_2^{\cdot -} \quad [6]$$

$$O_2^{\cdot -} + Fe^{3+} \rightarrow O_2 + Fe^{2+} \quad [7]$$

$$6OH^{\cdot} + W \rightarrow WO_3 + 3H_2O \quad [8]$$

$$W + O_2 \rightarrow WO_2 \quad [9]$$

$$2WO_2 + O_2 \rightarrow 2WO_3 \quad [10]$$

$$2WO_3 + 2(C_2O_4)^{2-} + O_2 \rightarrow 2WO_4{}^{2-} + 4CO_2 \quad [11]$$

First, the catalyst $K_3Fe(C_2O_4)_3$ is ionized to $3\,K^+$, Fe^{3+}, and $3(C_2O_4)^{2-}$ in the aqueous slurry at pH 2.3, as described in reaction 1. Then, the Fe^{3+} ions decompose the oxidant H_2O_2 to dissolved O_2, which is called a Fenton reaction, as described in reaction 2. Unlike reaction 2, in practice a Fenton reaction is a very complicated cycling decomposition process of H_2O_2 that is accelerated by very reactive radicals (i.e., $OH^{\cdot}$, $O_2^{\cdot -}$, and $HO_2^{\cdot}$), as shown in reactions 2–7. Thus, the dissolved O_2 as well as $OH^{\cdot}$ in the aqueous slurry oxidizes the W film surface, as described in reactions 8–10. Figure 4 shows evidence, obtained by XPS analysis, of oxidation on the W film surface. In addition, the dissolved $(C_2O_4)^{2-}$ ions simultaneously corrode the WO_3 layer on the W film surface by chemically changing $WO_4{}^{2-}$, as described in reaction 11 and shown by the Pourbaix diagram in Supplementary Fig. S4. The presence of $WO_4{}^{2-}$ on the W film surface could easily be confirmed by the zeta potential dependency of the WO_3 particles on the $K_3Fe(C_2O_4)_3$ concentration in Fig. 5a; that is, the zeta potential of the WO_3 particles became increasingly negative with increasing $K_3Fe(C_2O_4)_3$ concentration. From reactions 1–11, it is obvious that W-film CMP using slurry with the $K_3Fe(C_2O_4)_3$ catalyst simultaneously involves both chemical oxidation-dominant and corrosion-dominant

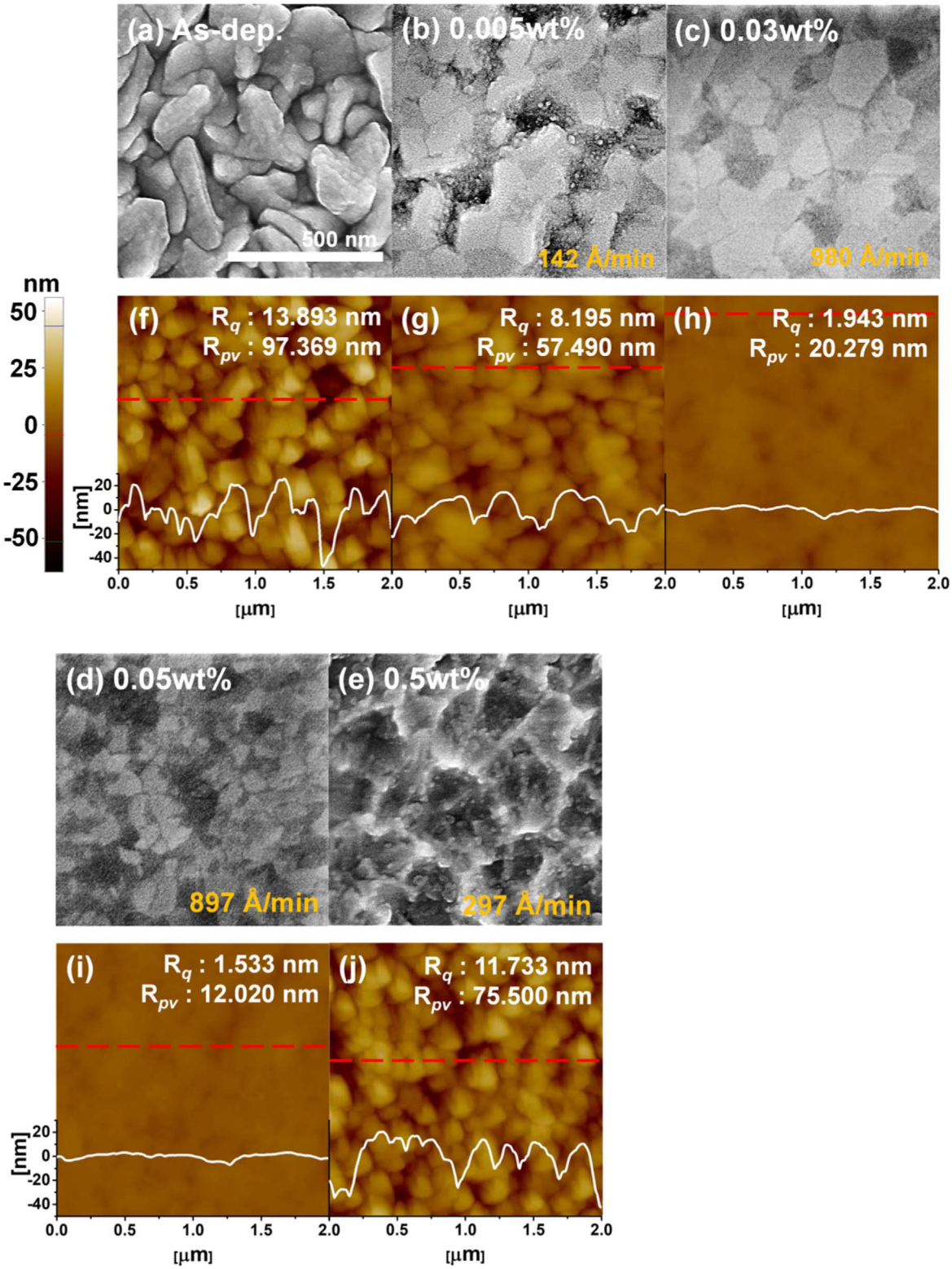

Figure 6. Surface morphology and roughness of W films after CMP, depending on the $K_3Fe(C_2O_4)_3$ concentration: SEM images for (a) the as-deposited condition, (b) 0.005 wt%, (c) 0.03 wt%, (d) 0.05 wt%, and (e) 0.5 wt%; and AFM images for (f) the as-deposited condition, (g) 0.005 wt%, (h) 0.03 wt%, (i) 0.05 wt%, and (j) 0.5 wt%. The SEM images were observed at 15 kV, while the AFM images were measured over a 2 μm $\times$ 2 μm scanning area.

mechanical planarization. Furthermore, the degree of dependency on the $K_3Fe(C_2O_4)_3$ concentration differs between the chemical oxidation-dominant mechanical planarization and the corrosion-dominant mechanical planarization. In the range of $K_3Fe(C_2O_4)_3$ concentration between 0.001 and 0.005 wt%, the degree of chemical oxidation- and corrosion-dominant mechanical planarization together is higher than that of the corrosion-dominant process alone. As a result, no evidence of corrosion on the W film surface was found after CMP, as shown in Figs. 6b and 7a. In comparison, in the $K_3Fe(C_2O_4)_3$ concentration range between 0.01 and 0.1 wt%, both processes were

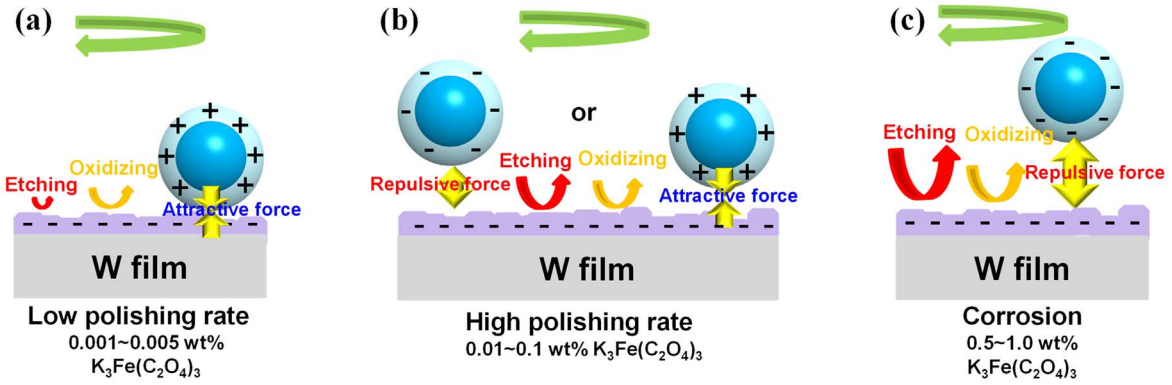

Figure 7. Schematic of the W-film polishing mechanism, depending on the $K_3Fe(C_2O_4)_3$ catalyst concentration. The arrow magnitudes indicate the degree of chemical oxidation (yellow: WO_3) and corrosion (red: WO_4^{2-}): (a) 0.001–0.005 wt%, (b) 0.01–0.1 wt%, and (c) 0.5–1.0 wt%.

enhanced. Nevertheless, the degree of chemical oxidation- and corrosion-dominant mechanical planarization together is still higher than that of the corrosion-dominant process alone, again resulting in no corrosion of the W film surface after CMP, as seen in Figs. 6c and 6d and Fig. 7b. In the concentration range between 0.5 and 1.0 wt%, however, the degree of corrosion-dominant mechanical planarization becomes rather higher than that of the chemical oxidation-dominant process, producing severe corrosion of the W film surface after CMP, as shown in Figs. 6e and 7c.

Moreover, the $(C_2O_4)^{2-}$ ions in the aqueous slurry are chelated on the positively charged nanoscale colloidal-ZrO_2 abrasives, whose zeta potential changed from a positive to a negative value when the $K_3Fe(C_2O_4)_3$ concentration increased, as shown in Fig. 5a. Note that the secondary ZrO_2 abrasive-size was almost independent of catalyst concentration, which would not affect the polishing rate of the W- and SiO_2-films as shown in Supplementary Fig. S3. Thus, during CMP, in region **I** [$K_3Fe(C_2O_4)_3$ concentration between 0.001 and 0.03 wt%], the attractive (negative) electrostatic force at the interface between the colloidal-ZrO_2 abrasives and the W film surface decreased with increasing $K_3Fe(C_2O_4)_3$ concentration. As a result, the W film rapidly increased with the $K_3Fe(C_2O_4)_3$ concentration, without the presence of corrosion on the surface, as shown in Figs. 1 and 5b. Otherwise, in region **II** [$K_3Fe(C_2O_4)_3$ concentration between 0.04 and 0.1 wt%], the repulsive (positive) electrostatic force at the interface between the ZrO_2 abrasives and the W film surface increased with the $K_3Fe(C_2O_4)_3$ concentration, so that the W film greatly decreased with the $K_3Fe(C_2O_4)_3$ concentration. In conclusion, then, the W-film CMP performance (i.e., the polishing rate and surface morphology) is determined by the different degrees of chemical oxidation-dominant and corrosion-dominant mechanical planarization, as well as by the electrostatic force at the interface between the colloidal-ZrO_2 abrasives and the W film surface during CMP, depending on the $K_3Fe(C_2O_4)_3$ catalyst concentration in the slurry.

Remaining colloidal-ZrO_2 abrasives on the film surface after CMP.—Finally, because the remaining colloidal-ZrO_2 abrasives on the W film surface after CMP cause scratches that are detrimental for a semiconductor device, we measured the dependency of the number of remaining colloidal-ZrO_2 abrasives on the W and SiO_2 film surfaces on the $K_3Fe(C_2O_4)_3$ concentration, as shown in Fig. 8. The number greatly decreased from 1152 to 311 when the $K_3Fe(C_2O_4)_3$ concentration increased from 0.001 to 1.0 wt%. This result can easily be analyzed by considering the electrostatic force at the interface between the ZrO_2 abrasives and the W film surface, in terms of the $K_3Fe(C_2O_4)_3$ concentration. In region **I** [$K_3Fe(C_2O_4)_3$ concentration between 0.001 and 0.03 wt%], because the attractive (negative) electrostatic force at the interface between the colloidal-ZrO_2 abrasives and the W film surface greatly decreased with increasing $K_3Fe(C_2O_4)_3$ concentration, the number of

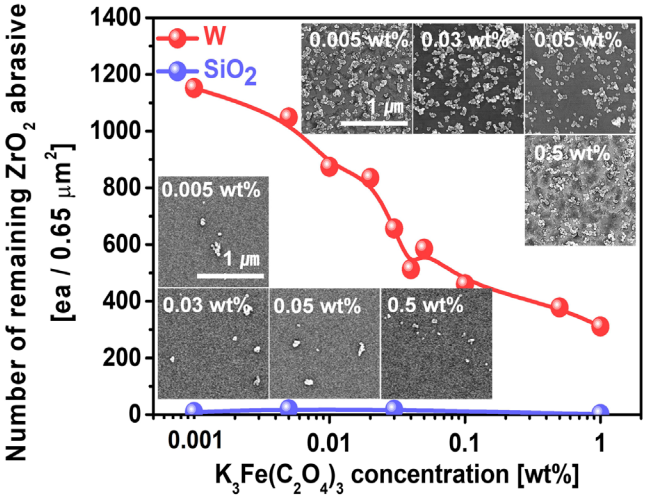

Figure 8. Dependency of the number of remaining ZrO_2 abrasives on the $K_3Fe(C_2O_4)_3$ catalyst concentration after the W-film CMP.

remaining colloidal-ZrO_2 abrasives on the W film surface remarkably decreased with increasing $K_3Fe(C_2O_4)_3$ concentration, as shown in Figs. 5b and 8. On the other hand, in region **II** [$K_3Fe(C_2O_4)_3$ concentration between 0.04 and 0.1 wt%], because the repulsive (positive) electrostatic force at the interface between the colloidal-ZrO_2 abrasives and the W film surface increased greatly with the $K_3Fe(C_2O_4)_3$ concentration, the number of particles remaining on the surface considerably decreased with increasing $K_3Fe(C_2O_4)_3$ concentration. The number of remaining colloidal-ZrO_2 abrasives on the SiO_2 film surface was not dependent, however, on the $K_3Fe(C_2O_4)_3$ concentration, because the magnitude of the electrostatic force at the interface between the colloidal-ZrO_2 abrasives and the SiO_2 film surface was relatively low (less than 10 in absolute value), as shown in Figs. 5 and 8.

Conclusions

In semiconductor device fabrication, the importance of W-film CMP has greatly increased, because the surface topography and the frequency of W-film CMP have rapidly increased as devices have been scaled down more and more. In W-film CMP, a Fenton reaction between a catalyst and an oxidant (i.e., H_2O_2) in an aqueous slurry is necessary for forming a nanoscale oxide layer on the W film surface after mechanical polishing at the interface between the abrasives and the surface. In particular, the catalyst and colloidal abrasive design of W-film CMP slurry has been a key research topic. Because it determines surface chemical and mechanical reaction at interface between W-film and nanoscale colloidal-ZrO_2 abrasives for CMP using $K_3Fe(C_2O_4)_3$ Catalyst. As a result, it decides the CMP

performance, including the polishing rate and selectivity, surface morphology (i.e., dishing and erosion), abrasive adsorption on the film, and slurry stability (i.e., agglomeration of abrasives with dissolved O_2 bubbles). In general, a lower catalyst concentration in W-film CMP slurry leads to better slurry stability.

Our proposed new catalyst, $K_3Fe(C_2O_4)_3$, and new nano-scale colloidal abrasive, ZrO_2, showed a specific W-film polishing-rate dependency on the catalyst concentration: specifically, the polishing rate peaked at a $K_3Fe(C_2O_4)_3$ concentration of 0.03 wt%, which is a considerably lower catalyst concentration as compared to $Fe(NO_3)_3$. In addition, two different W film surface morphologies were found after CMP: an chemically oxidized surface or a corroded surface, depending on the $K_3Fe(C_2O_4)_3$ concentration. We found that both chemical oxidation-dominant and corrosion-dominant mechanical planarization simultaneously occurred during W-film CMP. The dominant CMP mechanism was determined by the degree of difference between the chemical oxidation- and corrosion-dominant processes. At a low $K_3Fe(C_2O_4)_3$ concentration between 0.001 and 0.03 wt%, the W-film CMP mechanism was the oxidation-dominant mechanical planarization, generating no corrosion on the W film surface. In contrast, at a high $K_3Fe(C_2O_4)_3$ concentration between 0.03 and 1.0 wt%, the W-film CMP mechanism was the corrosion-dominant process, producing a corroded W film surface. Moreover, chelating of dissolved $(C_2O_4)^{2-}$ ions on the ZrO_2 abrasives and the W and SiO_2 film surfaces determined the electrostatic force at the interface between the abrasives and the film, which directly determined the polishing rate. Thus, the W-film polishing rate peaked at a specific $K_3Fe(C_2O_4)_3$ concentration, as did the SiO_2-film polishing rate. These results indicate that the surface chemical and mechanical reaction behavior of the $K_3Fe(C_2O_4)_3$ catalyst showed completely different behavior from that of another catalyst, $Fe(NO_3)_3$. Hence, $K_3Fe(C_2O_4)_3$ should be a very useful and powerful catalyst for W-film CMP of semiconductor devices below the 20-nm design rule, because it can give excellent W-film CMP performance with a remarkably low catalyst concentration.

Acknowledgments

This work was supported by the Republic of Korea's MOTIE (Ministry of Trade, Industry and Energy) (10085643) and KSRC (Korea Semiconductor Research Consortium) support program for the development of future semiconductor devices, and by the Brain Korea 21 PLUS Program.

ORCID

Jea-Gun Park https://orcid.org/0000-0002-5831-2854

References

1. M. Popovici et al., *IEEE Int. Electron Devices Meet.*, **2018**, 2.7.1 (2018).
2. K. Parat and A. Goda, *IEEE Int. Electron Devices Meet.*, **2018**, 2.1.1 (2018).
3. G. Bae et al., *IEEE Int. Electron Devices Meet.*, **2018**, 28.7.1 (2018).
4. T. N. Theis, *IBM J. Res. Develop.*, **44.3**, 379 (2000).
5. V. Kamineni et al., *Interconnect Technology Conference/Advanced Metallization Conference (IITC/AMC), IEEE*105 (2016).
6. T. S. Jang, M. S. Yoo, Y. T. Kim, S. Y. Cha, J. G. Jeong, and S. H. Lee, *2014 IEEE International Reliability Physics Symposium.*, **2014**, 4.1 (2014), 4.4.
7. F. B. Kaufman, D. B. Thompson, R. E. Broadie, M. A. Jaso, W. L. Gutherie, D. J. Pearson, and M. B. Small, *J. Electrochem. Soc.*, **138**, 3460 (1991).
8. Y. J. Seo, N. H. Kim, and W. S. Lee, *Mater. Lett.*, **60**, 1192 (2006).
9. R. Yagan and G. B. Basim, *ECS J. Solid State Sci. Technol.*, **8**, P3118 (2019).
10. A. Kargagoz, V. Craciun, and G. B. Basim, *ECS J. Solid State Sci. Technol.*, **4**, P1 (2015).
11. G. Lim, J. H. Lee, J. Kim, H. W. Lee, and S. H. Hyun, *Wear*, **257**, 863 (2004).
12. E. A. Kneer, C. Raghunath, S. Raghavan, and J. S. Jeon, *J. Electrochem. Soc.*, **143**, 4095 (1996).
13. J. H. Lim, J. H. Park, and J. G. Park, *J. Electrochem. Soc.*, **159**, H363 (2012).
14. Y. J. Seo and W. S. Lee, *Microelectron. Eng.*, **77**, 132 (2005).
15. E. A. Kneer, C. Raghunath, V. Mathew, S. Raghavan, and J. S. Jeon, *J. Electrochem. Soc.*, **144**, 3041 (1997).
16. G. Lim, J. H. Lee, J. W. Son, H. W. Lee, and J. Kim, *J. Electrochem. Soc.*, **153**, B169 (2006).
17. J. H. Lim, J. H. Park, and J. G. Park, *Appl. Surf. Sci.*, **282**, 512 (2013).
18. Y. J. Seo, N. H. Kim, and W. S. Lee, *Microelectron. Eng.*, **83**, 428 (2006).
19. P. Salgado, V. Melin, D. Contreras, Y. Moreno, and H. D. Mansilla, *J. Chil. Chem. Soc.*, **58**, 2096 (2013).
20. D. White, J. Parker, S. Li, and V. Dravid, *MRS Online Proceedings Library Archive***991** (2007).
21. Y. J. Seo, S. W. Park, and W. S. Lee, *IEEJ Trans. Electr. Electr.*, **7**, 108 (2006).
22. M. Ziomek-Moroz, A. Miller, J. Hawk, K. Cadien, and D. Y. Li, *Wear*, **255**, 869 (2003).
23. S. B. Akonko, D. Y. Li, M. Ziomek-Moroz, J. Hawk, A. Miller, and K. Cadien, *Wear*, **259**, 1299 (2005).
24. M. S. Lim, P. A. W. Heide, S. S. Perry, H. C. Galloway, and D. C. Koeck, *Thin Solid Films*, **457**, 346 (2004).
25. M. L. Kremer, *J. Phys. Chem. A*, **107**, 1734 (2003).
26. S. R. Pouran, A. A. A. Raman, and W. M. A. W. Daud, *J. Clean. Prod.*, **64**, 24 (2014).
27. P. V. Nidheesh, R. Gandhimathi, and S. T. Ramesh, *Environ. Sci. Pollut. Res.*, **20**, 2099 (2013).
28. Y. Sun and J. J. Pignatello, *J. Agric. Food Chem.*, **40**, 322 (1992).
29. Y. A. Jeong et al., *Microelectron. Eng.*, **218**, 111133 (2019).
30. D. Stein, D. L. Hetherington, and J. L. Cecchia, *J. Electrochem. Soc.*, **146**, 376 (1999).
31. V. S. Chathapuram, T. Du, K. B. Sundaram, and V. Desai, *Microelectron. Eng.*, **65**, 478 (2003).
32. M. Pourbaix, *National Association of Corrosion Engineers International, Houston, TX*, 139 (1974).
33. E. Patricka, M. E. Orazemb, J. C. Sanchezc, and T. Nishida, *J. Neurosci. Meth.*, **198**, 158 (2011).